# Functionally upgraded passive devices for seismic response reduction

Genda Chen*

*Center for Infrastructure Engineering Studies, Missouri University
of Science and Technology (formerly University of Missouri-Rolla), Rolla, Missouri, USA*

Lyan-Ywan Lu‡

*Department of Construction Engineering, National Kaohsiung First University of Science
& Technology, Kaohsiung, Taiwan*

**Abstract.** The research field of structural control has evolved from the development of passive devices since 1970s, through the intensive investigation on active systems in 1980s, to the recent studies of semi-active control systems in 1990s. Currently semi-active control is considered most promising in civil engineering applications. However, actual implementation of semi-active devices is still limited due mainly to their system maintenance and associated long-term reliability as a result of power requirement. In this paper, the concept of functionally upgraded passive devices is introduced to streamline some of the state-of-the-art researches and guide the development of new passive devices that can mimic the function of their corresponding semi-active control devices for various applications. The general characteristics of this special group of passive devices are discussed and representative examples are summarized. Their superior performances are illustrated with cyclic and shake table tests of two example devices: mass-variable tuned liquid damper and friction-pendulum bearing with a variable sliding surface curvature.

## 1. Introduction

Active control has been studied intensively since two decades ago (Soong 1990, Manjunath and Bandyopadhyay 2005). With a single actuator, an active control system can generate a significant control force for the improvement of the global behavior of a building or bridge system. However, the external power required to change an active system is often unavailable during a strong earthquake event. In addition to cost, the reliability and maintenance issues of a control system are two hurdles to be overcome in its practical applications.

*Professor and Interim Director, E-mail: gchen@mst.edu
‡Professor, E-mail: lylu@ccms.nkfust.edu.tw

Passive devices were introduced to engineering applications two decades ago (Soong and Dargush 1997, Syrmakezis, *et al.* 2006). In comparison with active control, passive devices can change the behavior of a controlled structure in relatively local areas; their application in the structure often appears in multiple units in order to effectively mitigate structural vibration. Since they require no external power and little maintenance after installation, passive devices have gained increasing acceptance in practice. However, although passive devices can be optimized to achieve a performance objective under a specific loading and environmental condition, they are not adaptive to external disturbances in a conventional sense. Therefore, passive devices are in many cases less effective than active control.

The trade-off between the required external power and performance of a control strategy has led to the development and extensive research of semi-active devices and systems (Ma and Ghasemi-Nejhad 2005, Batterbee and Sims 2005, Warnitchai and Hoang 2006, Maiti, *et al.* 2006, Samali, *et al.* 2006, Jung, *et al.* 2007). In this case, while the performance of a properly-designed semi-active device could be similar to that of an active control system, the power required to change the parameters of the device during an earthquake event is considerably lower, making it practical to use such a device in application. On the other hand, however lower the required external power is, semi-active systems need some maintenance over the years of their service.

In this paper, a suite of passive devices that can closely mimic the behavior of their corresponding semi-active devices are introduced. They have clearly-defined counterparts, conventional passive devices, but with superior performance in certain functions. As such, these systems are herein referred to as functionally upgraded passive devices. They require virtually no maintenance in applications and expect to gain wide acceptance in engineering practices. The new concept of these systems is illustrated with a mass-variable tuned liquid damper and a friction pendulum isolation bearing with a variable sliding surface curvature.

## 2. Functionally upgraded passive devices

Functionally upgraded passive devices include, but are not limited to, mass-variable tuned liquid dampers, friction pendulum bearings with variable sliding surface curvatures, friction-variable dampers with self-centering features, and nonlinear energy sink dampers. Their general characteristics are summarized below and exemplified with the listed examples.

### 2.1. General characteristics

Functionally upgraded passive devices introduced in this paper must be discussed with respect to conventional passive systems. They add one or more functions to their corresponding passive systems. In many cases, just like semi-active devices, they are adaptable to external disturbances as the main parameters of their corresponding conventional passive device change with the level of external excitations. A functionally-upgraded passive device has three general characteristics:

- It requires no external power to operate,
- It has a clearly-defined conventional passive device and adds at least one function to the passive device, such as adaptability to external disturbances and self-centering of friction dampers, and
- Its parameters can be automatically adjusted with the use of earthquake-induced energy and power.
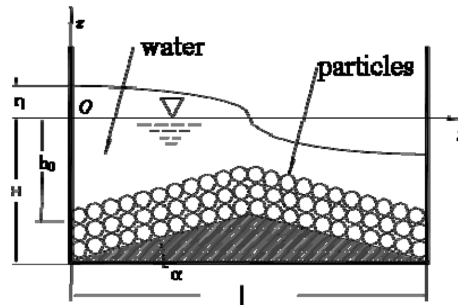
Fig. 1 Schematic view of a mass-variable tuned liquid damper

## 2.2. Mass-variable tuned liquid damper

A tuned liquid damper (TLD) has three undesirable characteristics. Like all tuned dampers, a TLD is generally ineffective in suppressing the first peak response of a building to impulsive loading (Soong and Dargush 1997). It is low in energy dissipation capability for the building structure being controlled. It has low damping so that, once in motion, the sloshing motion of a TLD continues after the earthquake excitation is over (Sun 1991). To overcome these undesirable features, a mass-variable tuned liquid damper (MVTLD) is introduced in this study.

An MVTLD can simply be constructed with a rectangular tank of sloped bottom (Xin 2006). As illustrated in Fig. 1, the tank is filled with water and fine sand particles. The sand particles are added to the water in the rectangular tank to increase the density of a mixture of sands and water after the sands are in a suspended state. The sloped bottom of the MVTLD is used to mimic the wave energy dissipating effect of a sloped beach (Reed, *et al.* 1998). More importantly, the sloped bottom of the tank can set sand particles in the tank in motion more rapidly when the tank is subjected to an increasing base excitation. As a result, the MVTLD has a larger liquid-tank contact area and a larger mass than a conventional tuned liquid damper (TLD) given the same space occupied by them.

Under a weak base excitation, the sand particles in the tank remain at the bottom of the tank and the water above is sloshing on the free surface. As the excitation increases, the sand particles appear in a liquefied state due to increase in pore pressure between the particles; the water and particles are sloshing together. Since the mass involved in sloshing increases with the base excitation, the proposed device is referred to as a mass-variable damper that requires no external energy. In terms of the requirements for mechanical and power services, it is a maintenance-free device.

## 2.3. Friction pendulum bearing with a variable sliding surface curvature

Friction pendulum system (FPS), as a sliding isolator, has been implemented in many existing structures (Mokha, *et al.* 1991). The sliding surface of a FPS isolator is in spherical shape so that the gravity load applied on the slider will provide a restoring stiffness and re-centering force for the isolated structure. Corresponding to the restoring stiffness, the isolated structure has a fixed natural period in second, depending upon the radius of the spherical sliding surface. As a result, FPS is sensitive to the long-period components in earthquake ground motions, such as near-field earthquake records (Hall, *et al.* 1995, Makris and Chang 2000). Indeed, the isolator displacement could be considerably amplified due to the long-period pulses present in most near-field ground motions (Jangid and Kelly 2001, Lu, *et*
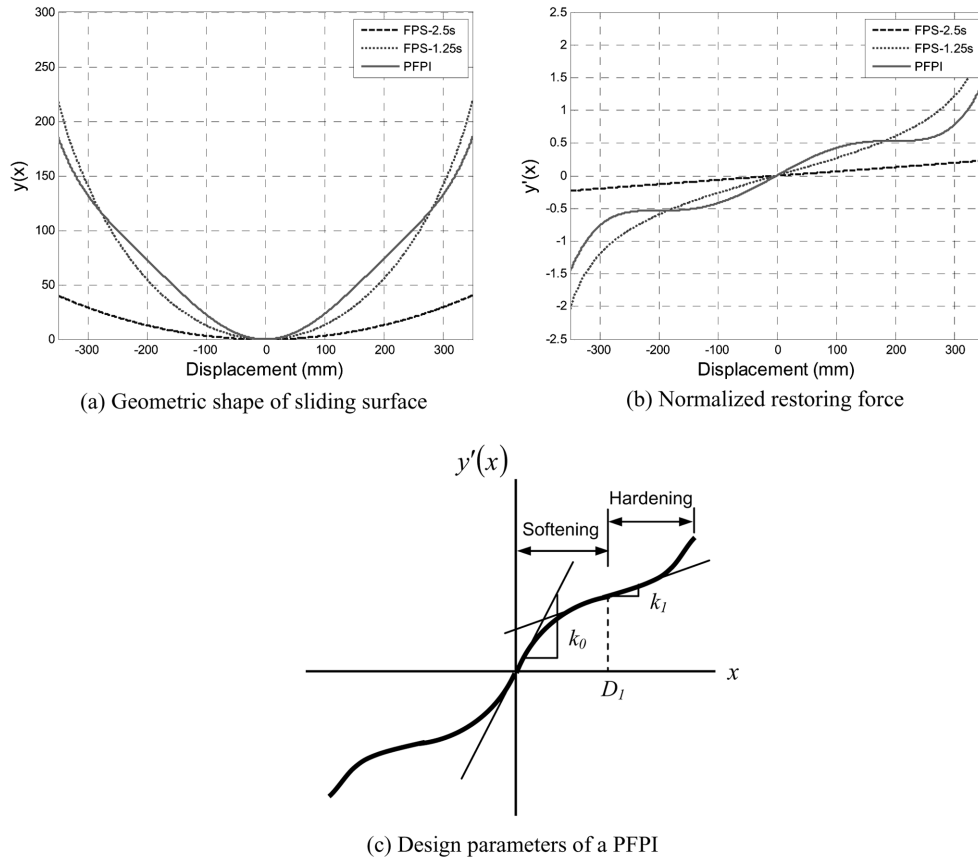
(a) Geometric shape of sliding surface            (b) Normalized restoring force



(c) Design parameters of a PFPI

Fig. 2 Comparison between an FPS and a PFPI

*al.* 2002, 2003). In order to prevent the potential resonance that an FPS may experience, a 6th order polynomial friction pendulum isolator (PFPI) with a variable characteristic period was introduced by Lu, *et al*. (2006).

As illustrated in Fig. 2(a), the sliding surface of a PFPI is axially symmetric about the centerline with variable curvatures. In addition, for the convenience of comparison, the elevation profiles of two FPS bearings, denoted by FPS-2.5s and FPS-1.25s, are also plotted in Fig. 2(a). The FPS-2.5s represents a FPS bearing with an isolation period of 2.5s, which is a commonly adopted period for FPS systems (Naeim and Kelly, 1999). On the other hand, the FPS-1.25s denotes a FPS with an isolation period of 1.25s, which represents a short-period isolator. The reason of showing FPS-1.25s is that its elevation is approximate to that of the PFPI at the same isolator displacement. The radii of the sliding surfaces for FPS-2.5s and FPS-1.25s are 1.55 m and 0.39 m, respectively. The seismic response the PFPI will be compared with those of the two FPS in a latter section. As shown in Fig. 2(a), the elevation profile of the PFPI is defined by a 6th order polynomial function. As a result, the slope $y'(x)$ of $y(x)$ in radial direction becomes a 5th order polynomial function of the displacement as shown in Fig. 2(b). The slope $y'(x)$ is also equal to the restoring force of the isolator normalized with respect to the isolator vertical load (Lu, *et al.* 2006). As illustrated in Fig. 2(b), the restoring force of the PFPI starts with a softening portion and is followed by a hardening portion. The softening portion functions as a base isolation

component for peak acceleration reduction in buildings while the hardening portion is to reduce the deformation of the isolator. Furthermore, as shown in Fig. 2(c), the restoring force of the PFPI can also be defined by three design parameters $k_0$, $k_1$, $D_1$: (1) the parameter $k_0$ defines the normalized initial stiffness at $x = 0$, i.e., $y''(0) = k_0$. (2) The parameter $D_1$ is a critical isolator displacement that defines the transition point between the softening and hardening behaviors. (3) The parameter $k_1$ defines the normalized isolator stiffness at the critical displacement $x = D_1$, i.e., $y''(D_1) = k_1$. The three design parameters for the PFPI shown in Fig. 2 are taken to be $k_0 = 5$ (1/m), $k_1 = 0$, $D_1 = 0.2$ m.

### 2.4. Friction-variable dampers

Friction is an effective way of energy dissipation that has been used in practice since ancient times. The amount of energy dissipation depends upon the clamped force and the sliding distance experienced between two rigid parts that can move against each other. To maximize the energy dissipation, the clamped force is typically set to high for strong earthquakes. Such a friction system, however, may dissipate zero energy since the two parts of the system may be stick to each other and experience no slippage under small or moderate earthquakes. This potential stick phase of a friction system usually results in sudden motions or jerks, which is harmful in building applications. Therefore, friction variable dampers are desirable for the mitigation of multiple earthquake hazard levels.

A friction-variable damper can be constructed with two steel plates clamped together by two parallel links whose ends are free to rotate but restrained for translational motions in all directions. The interface of the two plates is designed in a curved shape as shown in Fig. 3. As the top plate is moving against the bottom plate in either direction, the clamped force on the friction surface between the plates increased from two sources: elongation of the two clamping links and change in thickness of the two plates at the location of each link. When the links are elongated, the tension force in each link increases so that the clamped force applied on the friction surface increases. Similarly, the minimum thickness of the two plates is arrived at the initial position of the links. As the two plates move against each other, due to the curved friction surface, the plates at the location of links become thicker, resulting in further increase of the clamped force. Depending on the design of the curved shape of the fiction surface, various clamped forces as a function of the slip between the two plates can be generated. Although no external power required, the behavior of the friction damper is similar to a semi-active friction device such as piezoelectric friction dampers (Chen and Chen 2004a, 2004b).

Recently, self-centering features were introduced into friction damping devices (Zhang and Zhu 2006). They were realized by incorporating superelastic nitinol wire strands between two parts of a friction device. By changing the ratio between the yield strength of the nitinol wire strands and the friction between two parts, nearly self-centering performance of the friction device can be achieved. A similar concept can be introduced to the friction-variable damper schematically shown in Fig. 3 to add the self centering feature. The hysteresis loop of the friction damper illustrated in Fig. 3 depends on the shape of
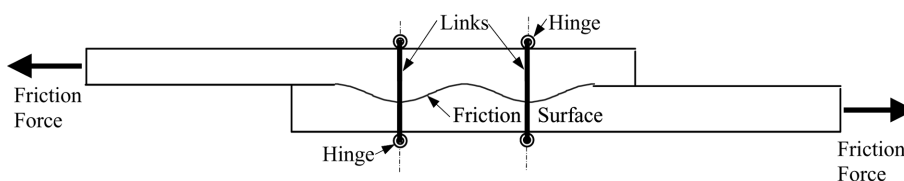


Fig. 3 Schematic view of a friction-variable damper

the friction surface. When the shape of the interface surface is defined by $y(x) = e|x(t)| + g|\dot{x}(t)|$ where $e$ and $g$ are two constants, the hysteresis loop is similar to those described in Chen and Chen (2004a, 2004b).

### 2.5. Nonlinear energy sink dampers

Tuned mass damper (TMD) has been applied to high rise buildings and bridges for the suppression of wind-induced vibration and other narrow frequency band vibration induced by machine operation and human walking. Earthquake loads, however, have a much wider band of frequency components. In this case, multiple TMDs have been considered to suppress several dominant modes of vibration (Chen and Wu 2001, 2003). In addition, after the earthquake excitation is over, part of the energy stored in the TMD during the earthquake may not be dissipated and instead imparted back to the building being controlled. This will cause unwanted vibration even after the earthquake.

Alternatively, a nonlinear TMD can be designed to widen the effective frequency band for earthquake applications. For this purpose, an "energy sink" device was proposed by Vakakis, *et al.* (2003). Functioning as a vibration absorber, the device is composed of a mass, a dashpot, and a nonlinear hardening or softening spring. Once installed on a primary structure (e.g. on top of a building), the device can rapidly and irreversibly absorb energy from the primary structure. The energy is actually dissipated without spreading back to the primary structure. Its performance is superior to the conventional TMDs (Vakakis, *et al.* 2003).

## 3. Proof-of-concept tests of an MVTLD

As the first example of the proposed functionally upgraded passive devices, the characteristics and validation of an MVTLD are discussed in greater details in this section. An emphasis is placed on the understanding of the motion of particles in a water tank and the shake table tests of mass-variable dampers for their seismic effectiveness in reduction of peak acceleration and story drift. The adaptability of the dampers to external excitations is of particular interests.

### 3.1. Experimental observations on particle motion in a water tank

To understand the behavior of particles in water, a 165-mm long rectangular tank made of plexiglass plates was built and tested on a small shaker under a horizontal harmonic excitation of 1.7 Hz. The plastic particles used in the tests had a specific weight of 1.2. Both a V-shaped and a W-shaped bottom of the tank were considered. The images corresponding to the peak displacement responses under various levels of excitation, represented by the shaker displacement amplitude, $d_{max}$, are presented in Fig. 4(a) for the V-shaped bottom and Fig. 4(b) for the W-shaped bottom to illustrate the mobilization process of the particles. These results clearly indicated that the mass of a mixed water and particles changes with the level of excitations. As the base excitation increases, more particles are mixed with the sloshing water. In this way, the concept of an MVTLD can be realized in applications. In comparison with the flat-bottom tank (not shown), the particles in the sloped-bottom tank are much easier to be lifted, particularly in the tank with the W-shaped bottom. This can be clearly observed in the case of $d_{max} = 20$ mm where particles for the W-shaped bottom surpassed over the apex of the triangle bottom.
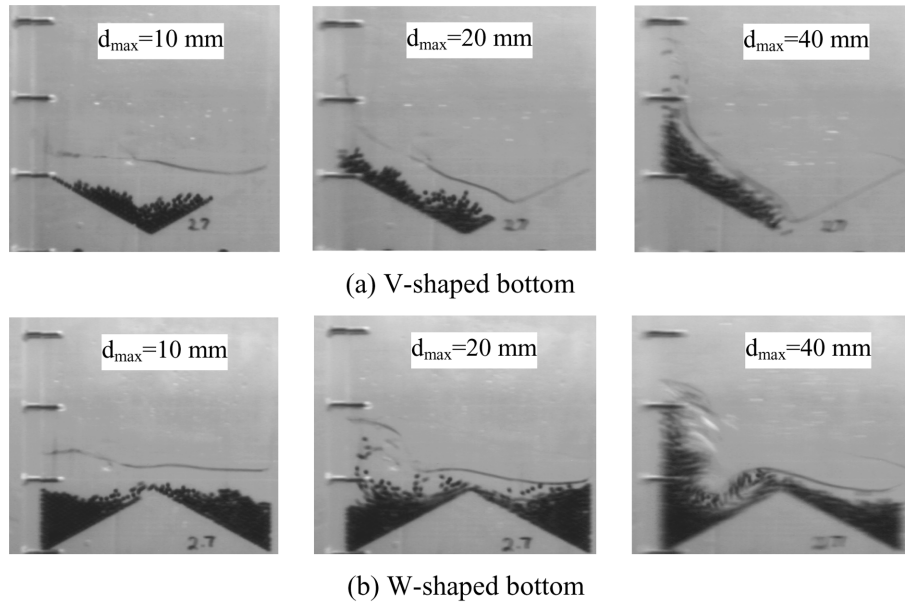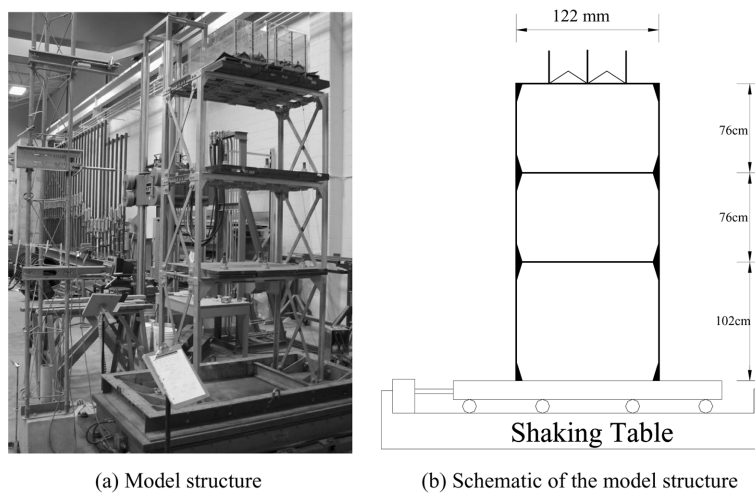
(a) V-shaped bottom



(b) W-shaped bottom

Fig. 4 Particle motion in a rectangular tank of sloping bottom

### 3.2. Shake table tests of a 3-story building frame with/without TLDs

The structure used for this experimental study is a 1/4-scale, three-story steel frame structure resting on the MTS shake table in the Highbay Structures Laboratory at the University of Missouri-Rolla. As shown in Fig. 5, the prototype structure is 1.22 m long, 0.61 m wide, and 2.54 m tall. The properties of the steel structure were identified with a series of shake table tests under harmonic loading (Xin 2006). The fundamental frequency and its corresponding damping ratio of the steel structure are 2.55 Hz and 0.52%, respectively.



(a) Model structure       (b) Schematic of the model structure

Fig. 5 Four TLDs installed on the 3rd floor of the 3-story steel frame

(a) Four TLDs           (b) An MVTLD of W-shaped bottom

Fig. 6 A rectangular tank with partition inserts

A 0.762 m×0.508 m×0.508 m water tank as shown in Fig. 6(a) was designed to mitigate the peak response of the 3-story steel frame as shown in Fig. 5. To enable the simulation both for a flat-bottom and a sloped-bottom shape, rigid bottom inserts were designed with movable configurations. The tank was installed on the third floor with three C-channels as a conventional or a mass-variable TLD device, depending on the content and the bottom shape of the tank. The tank was divided into four smaller tanks in the direction of loading, two pairs of two identical tanks (130 mm and 140 mm long) as indicated in Fig. 6(a), to tune the natural frequency of the water sloshing in two tanks to approximately 95% of the fundamental frequency of the steel structure, 2.55 Hz. An properly cut foam was inserted in the middle of the tanks, as illustrated in Fig. 6(b), to keep the total weight of the water-sand mixture in the mass-variable TLD system the same as that of the water in the regular TLD so that their performance can be compared on a common basis. The mass of any TLD is 1.6% of the mass of the building structure.

The calculated natural frequencies of various TLD configurations are listed in Table 1. As expected, the natural frequency of the water sloshing in a tank of W-shaped bottom is lowest, and that of the flat-bottom tank is highest.

To evaluate the proposed MVTLD, a far-field and a near-field historical record were used during the experimental study. The records used are the N-S component of the 1940 El Centro earthquake and the N-S component of the 1995 Kobe earthquake. Since the shake table has a maximum stroke of only ±25.4 mm, to generate significant structural responses for the control experiment, both earthquake records were compressed in time to make their dominant frequencies approximately equal to the fundamental frequency, 2.55 Hz, of the structure under consideration. The scale factors used were 1/2.091 for El Centro earthquake and 1/2.102 for Kobe earthquake.

Since the shake table input is a displacement signal in voltage, the two acceleration time histories must be converted to displacement time histories by double integrations with zero initial conditions. Note that a Butterworth high pass filter was used for acceleration and velocity functions in frequency domain. Furthermore, to investigate the adaptability of the proposed MVTLD system, two levels of

Table 1 Calculated natural frequencies of various TLD configurations

| Bottom shape \ Tank & length | TLD1 & 130 mm | TLD2 & 140 mm |
|---|---|---|
| Flat | 2.34 | 2.19 |
| V-shape | 2.28 | 2.13 |
| W-shape | 2.22 | 2.07 |

Table 2 Multi-level earthquake inputs

| Earthquake Level | El Centro | | Kobe | |
|---|---|---|---|---|
| | Stroke (mm) | Designation | Stroke (mm) | Designation |
| 1 (0.0973 g) | 14.0 | E1 | 6.48 | K1 |
| 2 (0.177 g) | 25.4 | E2 | 11.7 | K2 |

these earthquake inputs were designed as summarized in Table 2 to run the shake table. In the table, each earthquake is denoted by the first letter of its name and its intensity is represented by the numerical number following the designated letter. For example, E1 stands for the first level El Centro earthquake. Both peak acceleration and stroke are also specified in Table 2 for each earthquake.

### 3.3. Effectiveness of the MVTLD

Table 3 shows the peak acceleration reductions under various excitations. It can be seen from the table that the proposed MVTLD systems (V-shaped and W-shaped bottom) can substantially reduce the absolute floor acceleration of the frame structure. In comparison with the conventional TLD system, the MVTLD with the W-shaped bottom is equally effective under low excitations but significantly more effective under strong earthquake inputs. The MVTLD with the V-shaped bottom is also considerably more effective for strong earthquakes, but less effective for weak earthquakes since the V-shaped bottom is more difficult to get sand particles in motion. With the mass-variable strategy (W-shaped bottom), the floor acceleration of the structure was further reduced by 12.2% for the E2 excitation and 10.3% for the K2 excitation in comparison with the conventional TLD controlled responses.

As the excitation level increases, the nonlinearity of the conventional TLD device becomes more obvious. Therefore, the TLD effectiveness decreases. However, the mass-variable strategy alleviated the nonlinearity of water sloshing. Furthermore, the large excitation caused more sand particles lifted and increased the effective mass of the TLD device. Therefore, for MVTLDs, the control effect under high level excitations is even better than under low level excitations. This is a distinctive characteristic of a MVTLD from the conventional TLD.

### 3.4. Near-field versus far-field ground motion effects

Table 3 also indicates that, in all cases, the reduction at the 3$^{rd}$ floor acceleration is higher under the far-field El Centro earthquake. These results indicate that TLD is generally more effective for far-field ground motions than for near-field motions.

Due to its passive working mechanism, particularly for deep-water TLD, a TLD device needs some time to be set in motion before it becomes effective in vibration mitigation. As a result, a TLD device may not be able to reduce the first peak response due to impulsive loading, for example, earthquake-induced ground motions. Since the mass of sloshing motion is a critical factor for the required set-in-

Table 3 3$^{rd}$ floor peak acceleration reduction (%)

| Input | E1 | K1 | E2 | K2 |
|---|---|---|---|---|
| Conventional TLD | 16.4 | 15.2 | 10.7 | 9.8 |
| V-shaped MVTLD | 12.3 | 10.9 | 23.5 | 18.6 |
| W-shaped MVTLD | 16.4 | 14.1 | 22.9 | 20.1 |

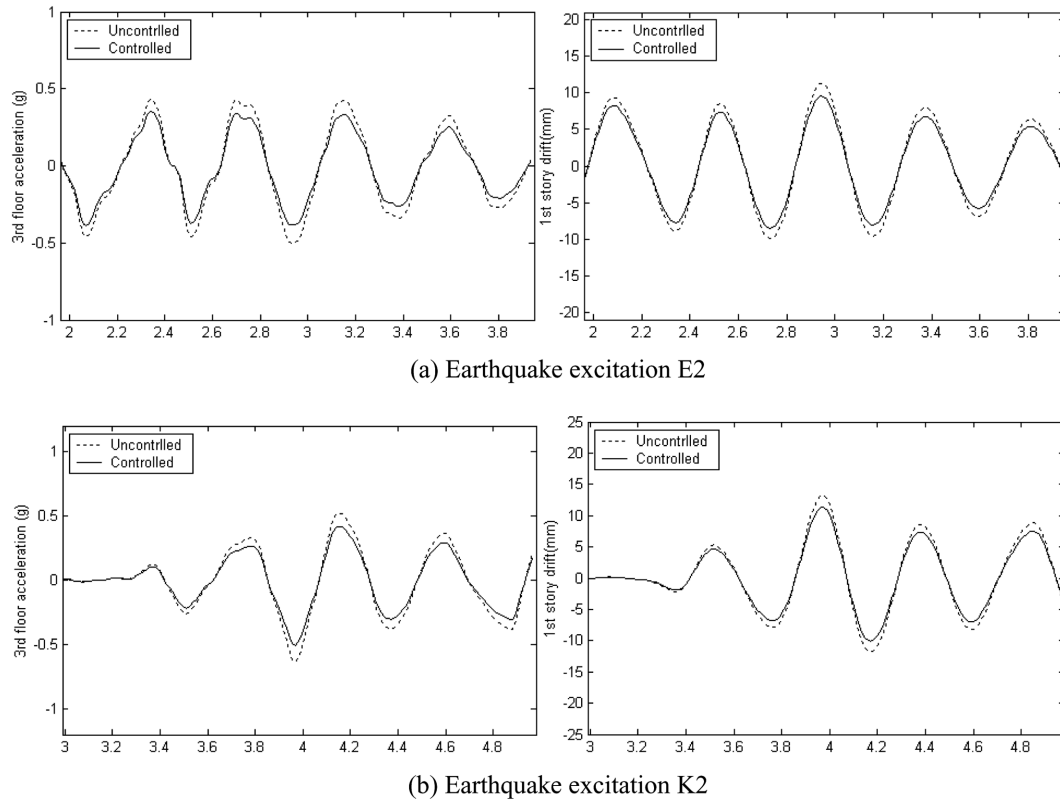(a) Earthquake excitation E2



(b) Earthquake excitation K2

Fig. 7 W-shaped bottom MVTLDs controlled versus uncontrolled structural responses

motion time, the proposed MVTLD is expected to perform better in terms of first peak reduction in comparison with the traditional TLD devices. This section is focused on the seismic effectiveness of the MVTLD of W-shaped bottom in first peak reduction of the earthquake-induced response. For this reason, only two seconds of time history responses spanning over the peak ground acceleration are presented in Figs. 7(a, b), corresponding to the high level of earthquakes. It is clearly shown that the reduction in peak acceleration and story drift is significant with the use of an MVTLD.

## 4. Proof-of-concept analysis and test of a PFPI

Near-field ground motions are mainly characterized with long-period velocity pulses. Depending on the shape of pulses, they can be classified as Type A, B, and C (Makris and Chang 2000). In this study, as shown in Fig. 8, a Type B acceleration pulse of a period of 2.5 sec. and the TCU075 earthquake record from the 1999 Chi-Chi Taiwan earthquake are applied to a single-story building to evaluate the performance of a PFPI system. The earthquake record presented in Fig. 8(b) was measured at a distance of 0.43 km from the tectonic fault. It includes a long-period pulse between 5 and 10 sec. According to Makris and Chang's classification, the Chi-Chi earthquake record can be classified as a Type B waveform with an approximate pulse period of 4.5 sec. Note that the peak ground acceleration of the Taiwan earthquake record was scaled into 0.4 g in the following analyses.
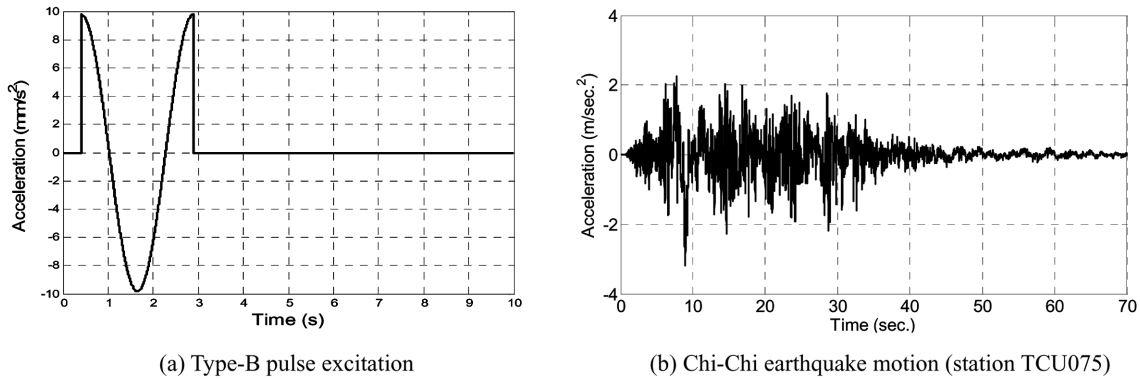
(a) Type-B pulse excitation

(b) Chi-Chi earthquake motion (station TCU075)

Fig. 8 Ground accelerations used in simulations: (a) Type-B pulse excitation, (b) Chi-Chi earthquake motion (station TCU075)

## 4.1. Numerical simulations on the seismic responses of a single-story building

As an example, a single-story building (floor weight = 300 tons and base weight = 100 tons) supported on two isolation bearings (Lu, *et al.* 2006) is considered here. The rigid-based building has a natural frequency of 1.67 Hz and a damping ratio of 5%. The coefficient of friction of all types of the bearings is taken to be 0.1. The design parameters of the PFPI shown in Fig. 2, i.e., $k_0 = 5$ (1/m), $k_1 = 0$, $D_1 = 0.2$ m, were used in the following simulation. In other words, the critical isolator drift of the simulated PFPI is set to be 0.2 m. The normalized initial stiffness and the stiffness corresponding to the critical isolator drift are equal to 5 1/m and 0, respectively. In the following, the seismic response of PFPI will be compared with those of the FPS systems shown in Fig. 2. Moreover, it should be noted that although the PFPI has a higher initial stiffness than that of the FPS (see Fig. 2(b)), it should not be classified as a short period structure, because the PFPI has no constant isolation period and has a softening behavior.
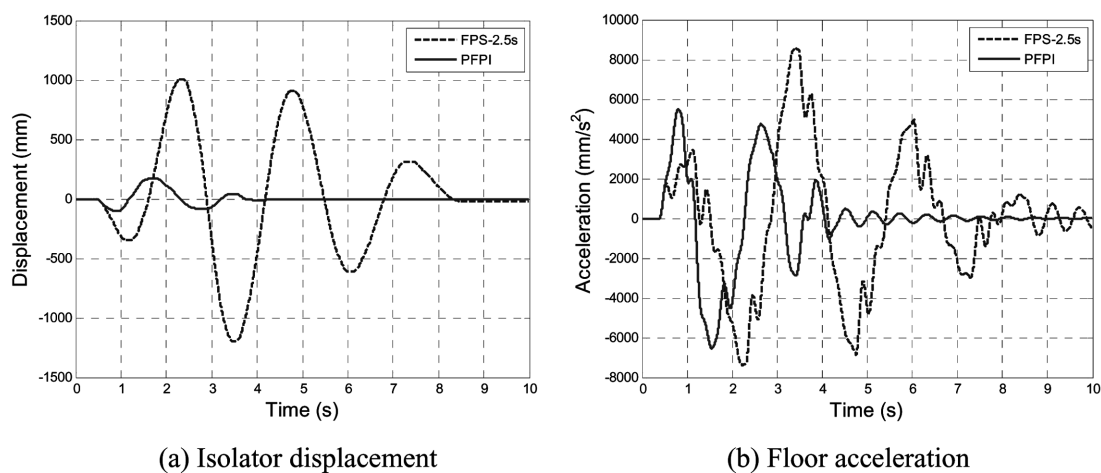


(a) Isolator displacement

(b) Floor acceleration

Fig. 9 Performance of PFPI and FPS bearings under Type-B pulse excitation (PGA=0.4g): (a) Isolator displacement, (b) Floor acceleration

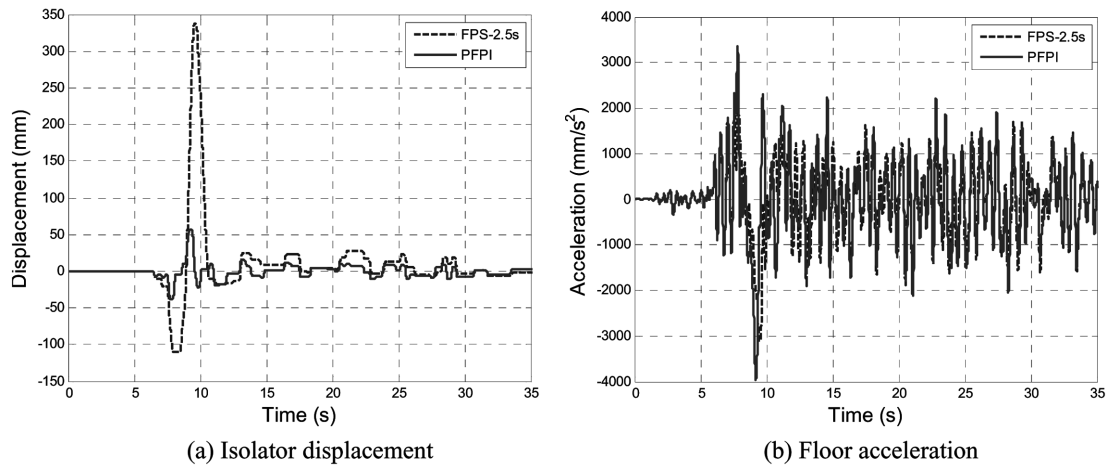(a) Isolator displacement

(b) Floor acceleration

Fig. 10 Performance of PFPI and FPS under Chi-Chi earthquake (PGA=0.4g): (a) Isolator displacement, (b) Floor acceleration

The time histories of the isolator displacement and the floor acceleration of the building are presented in Fig. 9(a, b) and Fig. 10(a, b) under the Type B pulse excitation and the Chi-Chi (station TCU075) ground motion, respectively. Fig. 9 shows that the FPS-2.5s has a peak acceleration response of as high as 0.8 g and an isolator displacement of 1 m. This implies that the FPS isolator is inefficient for an earthquake with a long-period pulse component. On the other hand, the PFPI improves the performance of the seismic isolation by reducing the peak acceleration to 0.5 g and the isolator displacement to 0.2 m. For the response of Chi-Chi earthquake, it is clearly observed in Fig. 10 that, in comparison with the FPS-2.5s, PFPI bearings significantly reduce the maximum isolator drift while they remain equally effective in suppressing the maximum floor acceleration. Specifically, under both excitations, the isolator drifts of the PFPI bearings are approximately 20% of the FPS isolator drifts. In addition, FPS-2.5s bearings exhibit more obvious oscillations in both acceleration and displacement time histories due



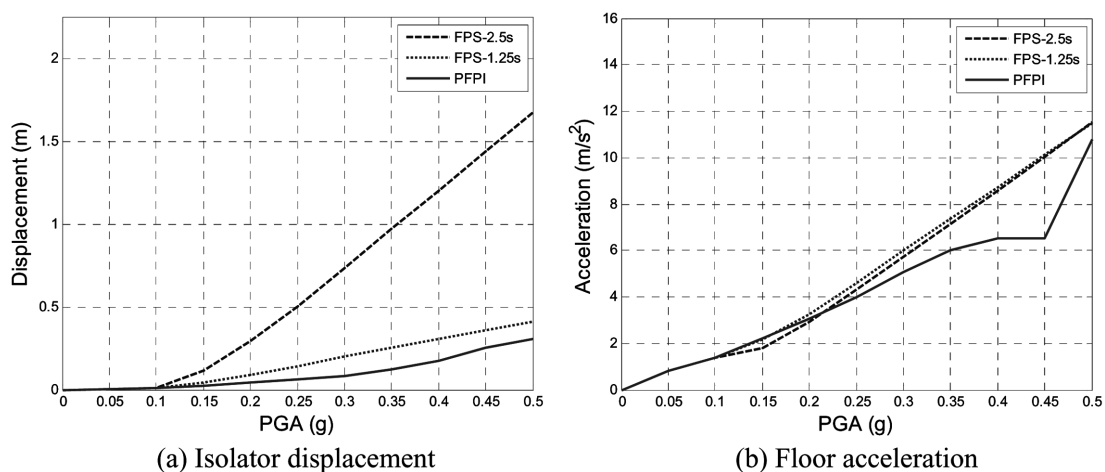(a) Isolator displacement

(b) Floor acceleration

Fig. 11 Comparison of peak responses due to Type-B pulse excitation with various PGA levels: (a) Isolator displacement, (b) Floor acceleration

to the pulse excitation.

When subjected to the Type B pulse excitation (see Fig. 8(a)) with different PGA levels, the peak responses of the PFPI, FPS-2.5s and FPS-1.25s bearings mentioned previously are simulated and compared in Fig. 11. Fig. 11 illustrates that at a higher PGA level between 0.25 g and 0.5 g, the PFPI has the lowest isolator displacement and structural acceleration responses, as compared with those of the FPS-2.5s and FPS-1.25s. In addition, Fig. 11 also shows that under a long-period pulse excitation, the short-period isolator FPS-1.25s performs better than FPS-2.5s in terms of the reduction of isolator displacement.

## 4.2. Cyclic tests of two PFPI bearings

To prove the concept of an isolation bearing with variable curvatures, cyclic tests were conducted. As shown in Fig. 12, a pair of PFPI bearings, detailed in Fig. 13, were fabricated and installed between two beams. The bottom beam was fixed to the floor through a braced frame structure while the top beam was allowed to move horizontally in parallel with the bottom beam. Two vertical hydraulic actuators were used to apply the compressive axial forces on the pair of PFPI bearings, and a third horizontal actuator was employed to apply a harmonic isolator displacement. A tri-axial load cell was installed under each PFPI bearing to measure the vertical and shear forces applied on the isolator. The design parameters of the PFPI bearings were taken to be: $k_0 = 3.8$ (1/m), $k_1 = 0$, and $D_1 = 0.08$ m. It should be noted that these parameters are different from those used previously in the simulation. As shown in Fig. 13, the PFPI bearings appear similar to a conventional FPS bearing. In direct contact with the sliding surface of the bearing, a steel slider of 35 mm in diameter was used in the test. Since the curvature of the sliding surface of the PFPI bearings changes with the sliding displacement, the friction material used at tip of the slider must be selected such that the slider can always remain in full contact with the sliding surface. For this purpose, a polymer material of desirable compressibility and ductility was used at the tip of the slider. The polymer material used in the test was ultra-high molecular weight polyethylene (UHMW-PE), which is a very common industrial material.

Each of the two bearings was subjected to a constant compressive load of 30 kN. A harmonic displacement loading of 0.01 Hz was then applied horizontally to the top beam of the test setup. The amplitude of the harmonic displacement gradually increases every three cycles. The experimental hysteresis loop of one PFPI bearing is depicted in Fig. 14(a). For comparison, Fig. 14(b) shows the theoretical hysteresis loop (Lu, *et al.* 2006). It can be observed from Fig. 14 that the experimental hysteresis loop
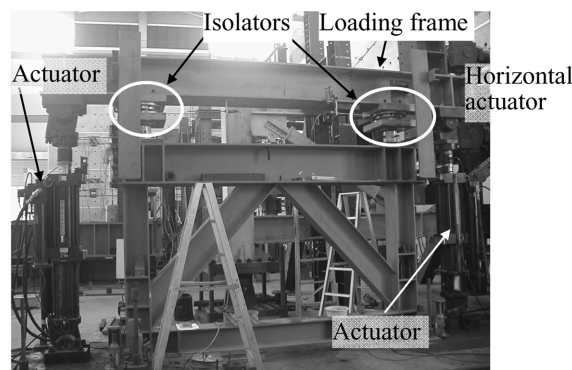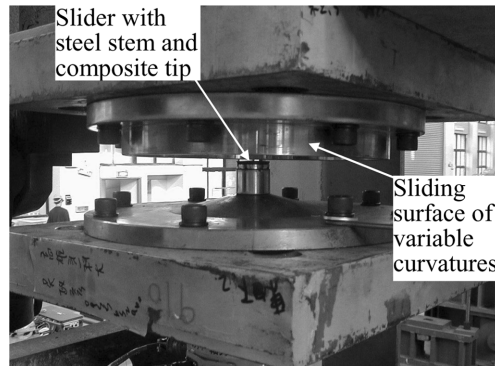


Fig. 12 Test setup of two PFPI bearings

Fig. 13 Details of a PFPI bearing



(a) Test data
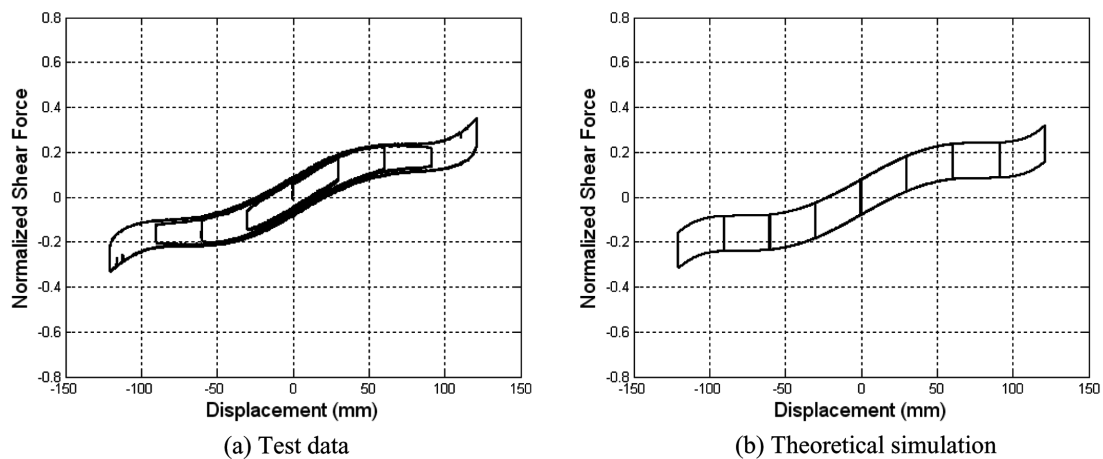
(b) Theoretical simulation

Fig. 14 Experimental versus theoretical hysteresis loops of a PFPI bearing: (a) Test data, (b) Theoretical simulation

of the prototype PFPI possesses a restoring-force curve defined by the 5th order polynomial function. The theoretical result matches fairly well with the experimental data.

Due to criticality of the friction material used at the tip of the slider, harmonic tests with a frequency of 0.4 Hz and a peak displacement of 50 mm were conducted to examine the stability and performance of the slider. In this test a constant compressive load of 20 kN was applied to each of the bearing. Fig. 15(a) shows the change of the friction with time, which was obtained from the tests under cyclic loading. The friction force was determined by subtracting the restoring force from the directly measured shear force of a PFPI bearing. The restoring force, as illustrated in Fig. 14, was evaluated from the directly measured compressive load applied on each bearing. Fig. 15(a) clearly indicates that the friction behaviour of the polymer material selected is very stable even when the curvature of the sliding surface of the PFPI dramatically changed with the isolator displacement. Fig. 15(b) depicts the relation between the coefficient of friction and the sliding velocity of the slider. The friction coefficient of the PFPI bearing is independent of sliding velocity up to 125 mm/s. In practice, the maximum sliding rate shall depend on the excitations and the design parameters of the PFPI. For examples, for the seismic responses shown in Fig. 10, the simulated peak sliding rates of the PFPI and FPS-1.25s are 380 mm/s and 146 mm/s, respectively.
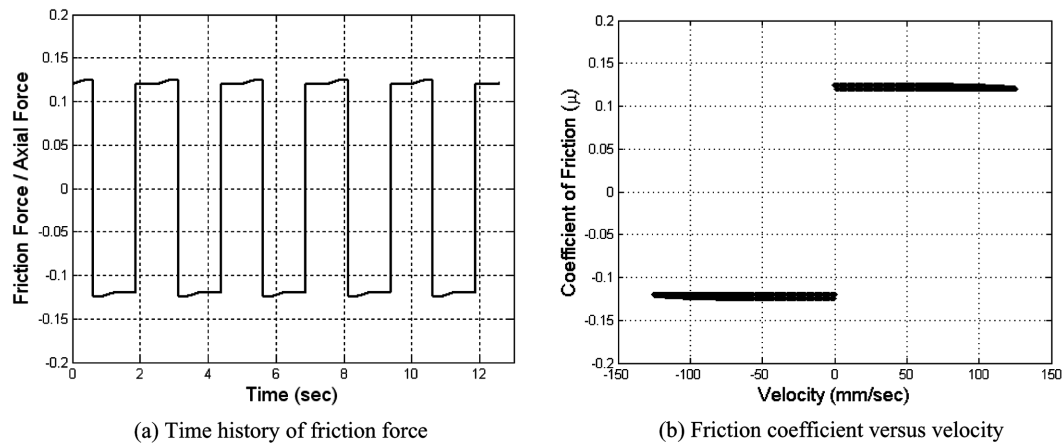
(a) Time history of friction force    (b) Friction coefficient versus velocity

Fig. 15 Friction behaviour of PFPI bearings (compressive load=20kN): (a) Time history of friction force, (b) Friction coefficient versus velocity

## 5. Conclusions

The concept of functionally upgraded passive devices has been introduced in this paper to streamline some of the state-of-the-art developments in structural control and guide the future developments of new passive systems. The general characteristics of these devices were presented and exemplified with four types of recently-proposed passive systems, including MVTLD systems, PFPI bearings, friction-variable dampers, and nonlinear energy sink dampers. The functions added to their corresponding conventional passive devices (TLD, FPS, friction dampers, and TMD) include the adaptability to external disturbances, self-centering feature of friction devices, first peak reduction ability, and frequency-independent suppression of both acceleration and displacement.

The performances of functionally upgraded passive devices were illustrated with the building tests of a MVTLD (shake table tests) and a PFPI (cyclic tests). The shake table test results have shown that the MVTLD can further reduce the building acceleration by more than 10% in comparison with its corresponding TLD due to increased mass in water sloshing motion by added particles. The new damper is adaptive to external excitations as the particles in water gradually become suspended. Such a damper requires no external power to operate and thus little maintenance during their life span, but it behaves like a semi-active system. Cyclic tests on two isolation bearings have indicated that the variable restoring force can be achieved with the concept of a PFPI. The friction materials selected for the PFPI bearings were stable and satisfactorily dissipated earthquake energy. Indeed, according to numerical simulations, the PFPI bearings can reduce the peak isolator displacement by 80% in comparison with a conventional FPS while both can effectively suppress the building acceleration.

## Acknowledgements

## References

Batterbee, D. C. and Sims, N. D. (2005), "Vibration isolation with smart fluid dampers: a benchmarking study", *Smart Struct. Sys.*, **1**(3), 235-256.

Chen, G. D. and Wu, J. N. (2001), "Optimal placement of multiple tuned mass dampers for reducing seismic responses of buildings", ASCE *J. Struct. Eng.*, **127**(9), 1054-1062.

Chen, G. D. and Wu, J. N. (2003), "Experimental study on multiple tuned mass dampers to reduce seismic responses of a three-story building structure", *Earthq. Eng. Struct. Dyn.*, **32**, 793-810.

Chen, G. D. and Chen, C. Q. (2004a), "Semi-active control of the 20-story benchmark building with piezoelectric friction dampers", ASCE *J. Eng. Mech.*, **130**(4), 393-400.

Chen, C. Q. and Chen, G. D. (2004b), "Shake table tests of a -scale three-story building model with piezoelectric friction dampers", *Struct. Control Health Monitoring*, **11**(4), 239-257.

Hall, J. F., Heaton, T. H., Halling, M. W. and Wald, D. J. (1995), "Near-source ground motions and its effects on flexible buildings", *Earthq. Spectra*, **11**, 569-605.

Jangid, R. S. and Kelly, J. M. (2001), "Base isolation for near-fault motion", *Earthq. Eng. Struct. Dyn.*, **30**, 691-707.

Jung, H. J., Choi, K. M., Park, K. S. and Cho, S. W. (2007), "Seismic protection of base isolated structures using smart passive control system", *Smart Struct. Sys.*, **3**(3), 385-403.

Lu, L. Y., Shih, M. H., Chang Chien, C. S. and Chang, W. N. (2002), "Seismic performance of sliding isolated structures in near-fault areas", *Proc. 7th US National Conference on Earthquake Engineering*, Session AT-2, July 21-25, Boston, MA, USA.

Lu, L. Y., Shih, M. H., Tzeng, S. W. and Chang Chien, C. S. (2003), "Experiment of a sliding isolated structure subjected to near-fault ground motion", *Proc. 7th Pacific Conference on Earthquake Engineering*, February 13-15, Christchurch, New Zealand.

Lu, L. Y., Wang, J. and Hsu, C. C. (2006), "Experiment and analysis of sliding bearings with variable frequency for near-fault seismic isolation", *Proc. 1st European Conf. on Earthq. Eng. Seis.*, Geneva, Switzerland, Sept. 3-8, Paper No. 183.

Ma, K. and Ghasemi-Nejhad, M. N. (2005), "Simultaneous precision positioning and vibration suppression of reciprocating flexible manipulators", *Smart Struct. Sys.*, **1**(1), 13-27.

Maiti, D. K., Shyju, P. P. and Vijayaraju, K. (2006), "Vibration control of mechanical systems using semi-active MR-damper", *Smart Struct. Sys.*, **2**(1), 61-80.

Makris, N. and Chang, S. P. (2000), "Effect of viscous, viscoplastic and friction damping on the response of seismic isolated structures", *Earthq. Eng. Struct. Dyn.*, **29**, 85-107.

Manjunath, T. C. and Bandyopadhyay, B. (2005), "Modeling and fast output sampling feedback control of a smart Timoshenko cantilever beam", *Smart Struct. Sys.*, **1**(3), 283-308.

Mokha, A., Constantinous, M. C., Reinhorn, A. M. and Zayas, V. A. (1991), "Experimental study of friction-pendulum isolation system", ASCE *J. Struct. Eng.*, **117**(4), 1201-1217.

Naeim, F. and Kelly, J. M. (1999), *Design of Seismic Isolated Structures: From Theory to Practice*, John Wiley & Sons.

Reed, D., Yu, J., Yeh, H. and Gardarsson, S. (1998), "Investigation of tuned liquid dampers under large amplitude excitation", ASCE *J. Eng. Mech.*, **124**(4), 405-413.

Samali, B., Wildjaja, J. and Rezes, J. (2006), "The controllable fluid dashpot damper performance", *Smart Struct. Sys.*, **2**(3), 209-224.

Soong, T. T. (1990), *Active Structural Control: Theory and Application*, John Wiley & Son, New York, NY.

Soong, T. T. and Dargush, G. (1997), *Passive Energy Dissipation Systems in Structural Engineering*, John Wiley & Son, NY.

Sun, L. M. (1991), "Semi-analytical modeling of tuned liquid damper (TLD) with emphasis on damping of liquid sloshing", Ph.D. Dissertation, University of Tokyo, Tokyo, Japan.

Syrmakezis, C. A., Mavrouli, O. A. and Antonopoulos, A. K. (2006), "Rehabilitation of hospital buildings using passive control systems", *Smart Struct. Sys.*, **2**(4), 305-312.

Vakakis, A. F., McFarland, D. M. and Bergman, L. A. (2003), "Vibration suppression by energy pumping", *Proc. US-Europe Workshop on Sensors and Smart Structures Technology*, Como and Somma Lombardo, Italy, 73-82.

Warnitchai, P. and Hoang, N. (2006), "Optimal placement and tuning of multiple tuned mass dampers for suppressing multi-mode structural response", *Smart Struct. Sys.*, **2**(1), 1-24.

Xin, Y. X. (2006), "Seismic performance of mass-variable tuned liquid dampers with particles fluidization in building applications", Ph.D. Dissertation, University of Missouri-Rolla, Rolla, USA.

Zhang, Y. F. and Zhu, S. (2006), "Seismic behavior of framed structure with self-centering damping braces", *Proc. 4th World Conf. on Struct. Control and Monitoring*, Paper No. 136, San Diego, CA.